AGU ADVANCING EARTH AND SPACE SCIENCES

Water Resources Research

RESEARCH ARTICLE
10.1029/2023WR035600

Generative Adversarial Network for Real-Time Flash Drought Monitoring: A Deep Learning Study

Ehsan Foroumandi[1], Keyhan Gavahi[1], and Hamid Moradkhani[1]

[1]Center for Complex Hydrosystems Research, Department of Civil, Construction, and Environmental Engineering, The University of Alabama, Tuscaloosa, AL, USA

Key Points:

- A new deep learning-based model using a generative adversarial network (GAN) is developed for real-time flash drought detection and monitoring
- Remote sensing maps are used as inputs to encompass the entire regions within the CONUS
- The proposed GAN is able to capture abrupt changes in drought patterns

Supporting Information:

Supporting Information may be found in the online version of this article.

Correspondence to:

E. Foroumandi and H. Moradkhani,
eforoumandi@crimson.ua.edu;
hmoradkhani@ua.edu

Citation:

Foroumandi, E., Gavahi, K., & Moradkhani, H. (2024). Generative adversarial network for real-time flash drought monitoring: A deep learning study. *Water Resources Research*, *60*, e2023WR035600. https://doi.org/10.1029/2023WR035600

Received 16 JUN 2023
Accepted 15 APR 2024

Abstract Droughts are among the most devastating natural hazards, occurring in all regions with different climate conditions. The impacts of droughts result in significant damages annually around the world. While drought is generally described as a slow-developing hazardous event, a rapidly developing type of drought, the so-called flash drought has been revealed by recent studies. The rapid onset and strong intensity of flash droughts require accurate real-time monitoring. Addressing this issue, a Generative Adversarial Network (GAN) is developed in this study to monitor flash droughts over the Contiguous United States (CONUS). GAN contains two models: (a) discriminator and (b) generator. The developed architecture in this study employs a Markovian discriminator, which emphasizes the spatial dependencies, with a modified U-Net generator, tuned for optimal performance. To determine the best loss function for the generator, four different networks are developed with different loss functions, including Mean Absolute Error (MAE), adversarial loss, a combination of adversarial loss with Mean Square Error (MSE), and a combination of adversarial loss with MAE. Utilizing daily datasets collected from NLDAS-2 and Standardized Soil Moisture Index (SSI) maps, the network is trained for real-time daily SSI monitoring. Comparative assessments reveal the proposed GAN's superior ability to replicate SSI values over U-Net and Naïve models. Evaluation metrics further underscore that the developed GAN successfully identifies both fine- and coarse-scale spatial drought patterns and abrupt changes in the SSI temporal patterns that is important for flash drought identification.

1. Introduction

Droughts are among the most harmful and pervasive environmental disasters that affect various natural processes and anthropogenic activities. Drought is a multifaceted phenomenon that can be categorized as agricultural, hydrological, meteorological, and socioeconomic droughts. Recent studies have illustrated that the frequency and intensity of droughts are increasing around the world, which has coincided with population growth and agricultural expansion, increasing the water demand manifold (Foroumandi et al., 2021, 2022a; Gavahi et al., 2020; Hammond et al., 2022; Madadgar & Moradkhani, 2014; Nourani et al., 2022; Xu et al., 2020; Zarekarizi et al., 2021). While drought is generally described as a slow-developing hazardous event (Wilhite et al., 2007), recent studies have revealed a rapidly developing type of drought, the so-called flash drought. Flash droughts usually begin with meteorological droughts and then transfer to agricultural droughts as the situation continues to deteriorate (Christian, Basara, Otkin, & Hunt, 2019; Otkin et al., 2018). Although precipitation deficit is the basic requirement for drought development, the rate of development and the ultimate severity are influenced by other variables (Edris et al., 2023; Madadgar & Moradkhani, 2013a). For example, when below-normal precipitation is combined with above-normal temperature, evaporation, winds, and so on, drought severity can rapidly increase.

Flash drought detection and monitoring are critically important because drought intensification may occur regardless of past or current moisture conditions. This dramatic situation has happened several times across the CONUS in recent years. For example, according to the U.S. Drought Monitor (USDM) in 2012, precipitation deficits were accompanied by abundant sunshine and above-normal temperature records across the central CONUS. In almost 2 months, different regions in this area experienced a three-to five-category increase in drought severity (Christian, Basara, Otkin, & Hunt, 2019). The southeastern CONUS encountered a similar condition in 2016 when during the fall, a large portion of the region experienced up to four category drought severity increments. Both flash droughts in 2012 and 2016 induced harmful impacts on the agricultural sector, with losses estimated at over $30 billion (Otkin et al., 2019). In 2017, the northern Great Plains flash drought, which is identified as the most destructive drought in decades, started in spring and evolved rapidly over the summer. Agricultural losses related to this drought were more than $2.6 billion in the US alone. Therefore,

developing models that are sensitive to abrupt changes in spatiotemporal drought patterns and can provide real-time drought maps will be of great use.

Flash droughts rapidly intensify drought conditions within a short time frame. To characterize the dynamics of flash droughts, various indices have been suggested and employed in prior studies. For example, the QuickDRI (Quick Drought Response Index), which was introduced by the National Drought Mitigation Center and the Center for Advanced Land Management Information Technologies at the University of Nebraska, is a machine learning-driven model proposed to identify rapidly fluctuating drought conditions (Chen et al., 2019). Ford and Labosier (2017) offered a perspective, defining flash drought based on the quick transition into agricultural drought conditions using the Soil Moisture Percentiles Drop methodology. Furthermore, Anderson et al. (2016) used the Evaporative Stress Index (ESI)—a metric for agricultural drought—to study flash droughts in Brazil. A novel index, called the Soil Moisture Volatility Index, was also proposed, demonstrating its efficacy in capturing the onset of flash droughts across both humid and semi-arid landscapes in comparison to some alternate approaches (Osman et al., 2021). Pertinently, previous studies have underscored the robustness of indices rooted in soil moisture when studying flash drought events (Sehgal et al., 2021; Tyagi et al., 2022).

The primary emphasis in drought monitoring is on various classifications determined by indicators calculated through either physically-based or statistical models (Ahmadalipour et al., 2017; Madadgar & Moradkhani, 2013b). These indicators serve as the basis for various studies that seek to predict drought severity and patterns. Additionally, other studies have attempted to overcome the drawbacks of traditional drought monitoring approaches. For example, Ahmadalipour and Moradkhani (2017) conducted a study that analyzed the uncertainties in observation data by employing hydrological modeling, with a particular focus on addressing the uncertainties associated with drought monitoring. Yan et al. (2018) presented a land data assimilation (DA) system to improve drought monitoring skills by merging remotely sensed soil moisture products. Xu et al. (2020) used an evolutionary particle filter approach to assimilate soil moisture data into a hydrologic model to study agricultural drought over the CONUS. Gavahi et al. (2022) employed two precipitation datasets provided by the North American Land Data Assimilation System (NLDAS) and Integrated Multi-satellite Retrievals for GPM (IMERG) to generate a more accurate Standardized Soil Moisture Index (SSI) product using a multivariate DA system. While physically-based models provide reliable results, certain limitations may impede their applicability in drought monitoring, especially in flash drought identification. Many of these techniques require significant computational power and suffer from higher latencies (in some cases exceeding a month) stemming from the input data lag. Furthermore, assimilating observational data into the models imposes a significant computational load (De Lannoy et al., 2022; Gavahi et al., 2022). Yet, for flash drought identification, real-time monitoring is crucial given the rapid shifts in its patterns.

Machine learning models have also been used in drought monitoring owing to their specific features including fast development time, and high generalization ability (Karamouz et al., 2022; Mokhtar et al., 2021; Sharghi et al., 2022). Different machine learning methods such as Artificial Neural Networks (ANN) (Foroumandi, Nourani, & Kantoush, 2022), Support Vector Regression (SVR) (Khan et al., 2020), and Random Forest (RF) (Zarei et al., 2022) have been used for drought-related research. Deep Learning (DL) models have also been used for drought monitoring due to their ability to handle large datasets and provide more accurate results. For example, Xiao et al. (2019) combined the Long Short-Term Memory (LSTM) and AdaBoost ensemble learning model to predict short and mid-term sea surface temperature for drought analysis. Kaur and Sood (2020) showed that a deep neural network model outperformed an optimized version of an SVR and an ANN that used a genetic algorithm in predicting drought conditions in different climates and time frames. Liu et al. (2021) used a U-Net model to segment a drought area and distinguish the severity of drought by using remote sensing images. Foroumandi et al. (2023) used DL techniques for pre-processing the GRACE-derived gridded data and then compared the performances of ANN, RF, and ConvLSTM models in downscaling the data for drought monitoring. While DL techniques have revolutionized various fields, they have been rarely employed in the domain of flash drought monitoring which suggests a possible avenue for research where DL can be introduced to improve prediction and understanding of these rapid onsets of drought events (Tyagi et al., 2022).

Generative Adversarial Network (GAN) proposed by Goodfellow et al. (2014) is a robust generative network that uses a flexible machine learning-based architecture. GAN is introduced to automatically learn patterns in the input domain and use those patterns to generate outputs. In other words, the network replicates the data distribution and generates target data. However, in other machine learning models, the model aims to learn a function that converts

the input to the target. GAN offers a distinct advantage over traditional DL models. Notably, GANs possess a mechanism that adaptively modifies its loss function in response to target data, facilitating the distinction between real and synthetic outcomes. Simultaneously, within this network, a secondary model is trained to produce results. This dual-model structure is a pivotal feature that underscores the uniqueness and efficacy of GANs in various applications. The GANs have been used in different fields over the years, such as audio enhancement (Su et al., 2021), medical imaging (Iqbal & Ali, 2018), hydrogeology (Chen et al., 2022), energy data generation (Li et al., 2022), and image manipulation (Minh Ngô et al., 2022).

In this study, using remotely sensed images, we develop the first GAN for flash drought monitoring. The network contains two deep learning models as the generator and discriminator of the network. One of the main advantages of the developed network, distinguishing it from conventional DL models, is its adaptive loss function that changes with respect to the network's efficacy. This eliminates the necessity for crafting specialized loss functions unique to distinct problems or regions, optimizing overall network performance. Additionally, the loss function is a combination of adversarial loss with other prevalent loss functions. Such inclusion of adversarial loss nudges the network to account for interdependencies among adjacent regions during the modeling phase. The adversarial training process in GANs serves as a form of implicit regularization, a particularly important process when dealing with limited or noisy datasets. Such a regularization contributes to improved generalization of the model to unseen data, vital for flash drought monitoring. The proposed network is trained and tested based on SSI over the CONUS for real-time flash drought monitoring. The model's efficiency is then compared with a U-Net model and a Naïve model.

2. Data

2.1. Datasets

The first phase of NLDAS forcing data (NLDAS-1) was initiated to couple atmosphere-land-ocean models to improve weather and seasonal climate predictions (Mitchell et al., 2004). The NLDAS produces Land Surface Model (LSM) forcing data, including meteorology reanalysis, gauge-based precipitation, and shortwave radiation. The second phase of the NLDAS model (NLDAS-2) applies some corrections to the gauge precipitation data and contains several enhancements to the equations and calibration of LSM (Peters-Lidard et al., 2011). The NLDAS-2 forcing data provides hourly maps at 0.125-degree spatial resolution from 1979 to the present. This study uses daily Evapotranspiration (ET), Soil Moisture (SM), Temperature (T), and Leaf Area Index (LAI) products of NLDAS-2-Noah from 2016 to 2020 as inputs to the model. These inputs are selected after performing feature selection on all NLDAS-2-Noah components. The feature selection is performed using a subset selection method with a forward stepwise approach. In this method, the goal is to find the best input data that contains the least dimension that most contributes to the model accuracy (Hastie et al., 2020). Data is downloaded from NASA's website providing LDAS datasets (https://ldas.gsfc.nasa.gov/nldas/nldas-2-model-data).

Recently, Gavahi et al. (2022) used the DA technique to produce daily SSI maps over the CONUS, which have been shown to have more reliable drought characterization compared to their counterparts. However, the product experiences a delay of 21 days, and the method requires significant computational resources. Consequently, this data collection is not appropriate for immediate decision-making or rapid analysis of flash drought occurrences. In this research, the daily SSI maps from 2016 to 2020 serve as both the targets and inputs. The selection of 2016–2020 as the timeframe for this study is due to the availability of the SSI maps exclusively for these years. Consequently, employing a GAN would be advantageous in managing the limited size of the data.

2.2. Data Preprocessing

In this study, daily ET_t, SM_t, T_t, and LAI_t, maps are used as inputs. On the other hand, the targets of the network are SSI_t maps. The following approach is employed for this purpose:

$$SSI_t = GAN(SSI_{t-21}, ET_t, SM_t, T_t, LAI_t) \quad (1)$$

The decision to use "21" in SSI_{t-21} is based on the 21-day latency observed in the target data collection, as mentioned earlier. By incorporating this lag period into the network, the resulting outputs will account for and cover the delay in the target data collection.

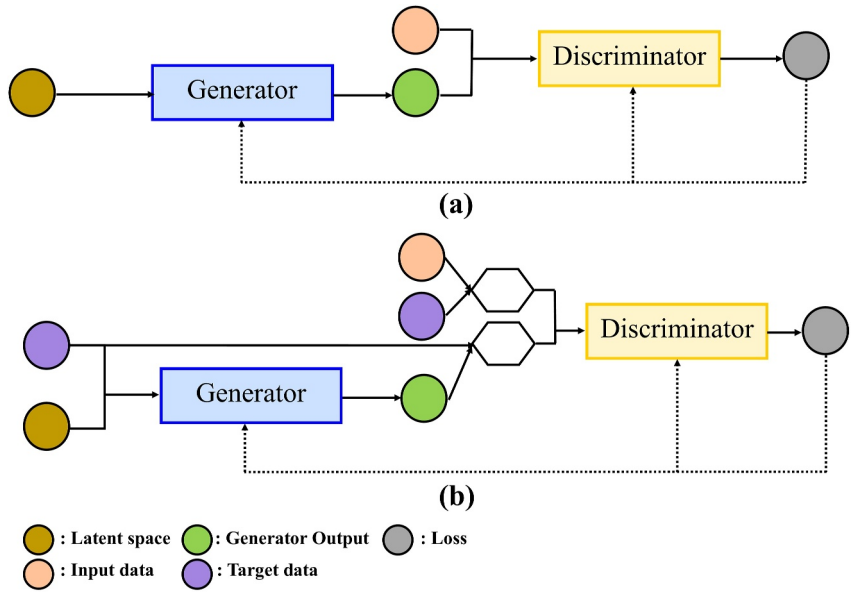

Figure 1. This figure presents a general architecture of (a) GAN, and (b) CGAN. Unlike a conventional GAN, in CGAN, both the generator and discriminator observe the target data. Latent Space is a lower-dimensional representation of high-dimensional data.

In total, about 7,312 daily NLDAS-2 maps and 1,828 daily SSI maps from 2016 to 2020 are collected and masked over the CONUS. The maps are randomly selected for training, validation, and testing procedures. The maps are normalized by subtracting the mean and dividing by the standard deviation. The mean and standard deviation are scalars calculated for the training dataset and used to normalize training, validation, and testing data. Zero padding, the process of adding zeros to the rows and columns of maps to preserve the spatial dimensions of the maps before applying the following operations, is applied to the maps and the final map size for both inputs and targets is 512×512.

3. Materials and Methods

3.1. GAN

The primary objective of this study is to develop a GAN for daily flash drought monitoring using the SSI index across the CONUS in real time. GANs work based on a game between two models, one called the "generator", and the other player is the "discriminator". The generator model is responsible for producing synthetic data, while the discriminator model assesses the accuracy of the generated outputs. By continually evaluating the discriminator's feedback, the generator model improves its ability to generate more realistic and accurate synthetic data. In the GAN framework, the discriminator model acts as a classifier with the objective of distinguishing between the synthetic data generated by the generator and real data. The outputs produced by the discriminator serve as a component of the loss function for the generator. This adversarial training process forms a minimax game, where both models strive to minimize their cost functions. Over time, the generator becomes better at producing realistic data, while the discriminator becomes better at identifying synthetic data.

Following the success of GANs in generating realistic data distributions, researchers aimed to have a more controlled generation process (Antipov et al., 2017). Conventional GANs lacked the ability to condition the generated output on certain desired attributes. To address this, Conditional GANs (CGANs) were proposed. The main idea behind CGANs is to provide both the generator and the discriminator with additional conditional information, usually in the form of a label or some other kind of auxiliary data (Elaraby et al., 2022). Figure 1 presents a general architecture for a GAN and a CGAN.

In this study, a CGAN is developed for flash drought monitoring; hereafter, it will be referred to as Drought GAN (DroGAN). The discriminator and generator architectures of DroGAN are adapted from Isola et al. (2017) and

Table 1
The SSI-Based Drought Classification Based on USDM Drought Categories

SSI values	Drought category	Notation
SSI ≥ −0.49	Normal or wet conditions	None
−0.79 ≤ SSI ≤ −0.5	Abnormally dry	D0
−1.29 ≤ SSI ≤ −0.8	Moderate drought	D1
−1.59 ≤ SSI ≤ −1.3	Severe drought	D2
−1.99 ≤ SSI ≤ −1.6	Extreme drought	D3
−2.0 ≥ SSI	Exceptional drought	D4

Radford et al. (2015). DroGAN employs a modified version of the U-Net model as its generator. Additionally, a Markovian discriminator is used as the discriminator component.

To generate flash drought maps using DroGAN, the outputs, which are SSI maps, are then categorized according to the specifications outlined in Table 1.

3.2. Generator (U-Net)

In this study, a modified version of the U-Net model is employed as the generator in the network. The purpose of this modified U-Net is to process maps as inputs and generate output maps as well. The utilized U-Net model in this study contains skip connections added between the *n*th layer and the (N-n)th layer, where *N* is the total number of layers in the U-Net (Xu et al., 2021). Figure 2 presents the architecture of a U-Net model which allows low-level (highly local features) information to shortcut across the model.

U-Net is a neural network model consisting of two paths. The first path, known as the analysis path or the contracting path, is similar to a convolutional neural network (CNN) layer and extracts information from the input maps. The second path which is known as the synthesis path or the expansion path consists of up-convolutions, allowing the network to learn the localized information. The skip connections allow concatenation between the maps in a step of the contracting path and a similar step of the synthesis path, helping to avoid the gradient vanishing problem (Siddique et al., 2021). The modified U-Net model consists of standardized single 2D convolution and 2D transpose-convolution blocks with batch normalization, dropout, and activation functions installed on them. Srivastava et al. (2014) showed that the dropout method considerably improves the performance of the network compared to other regularization techniques. In addition, in the modified version of the U-Net model, the input image goes down to the bottleneck until it reaches a one-by-one feature map and then, the upsampling process starts. This modification helps the model fully extract the features in the input domain. The textual summary of the generator model is tabulated in Table S1 in Supporting Information S2.

3.3. Markovian Discriminator (PatchGAN)

The Markovian discriminator (PatchGAN) is used as the discriminator model to penalize at the scale of patches. The PatchGAN operates convolutions across the images, aggregating the patch responses to produce the discriminator's final output, which is commonly referred to as adversarial loss. The PatchGAN discriminator categorizes sections of maps as "real" or "synthetic". Such a discriminator is often referred to as a Markovian discriminator, given its approach of representing the image as a Markov random field (MRF), where there is an assumption of independence for pixels distanced more than a patch's diameter from one another (Li & Wand, 2016). The PatchGAN discriminator is essentially a convolutional neural network designed to receive an

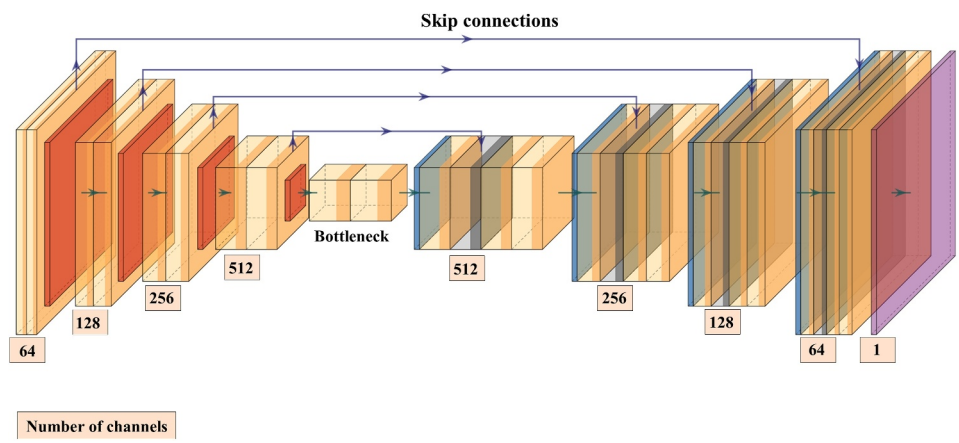

Figure 2. The architecture of a U-Net model. The input shape to the generator has the dimension of (5 × 512 × 512). This figure is plotted using the PlotNeuralNet code (Iqbal, 2018).

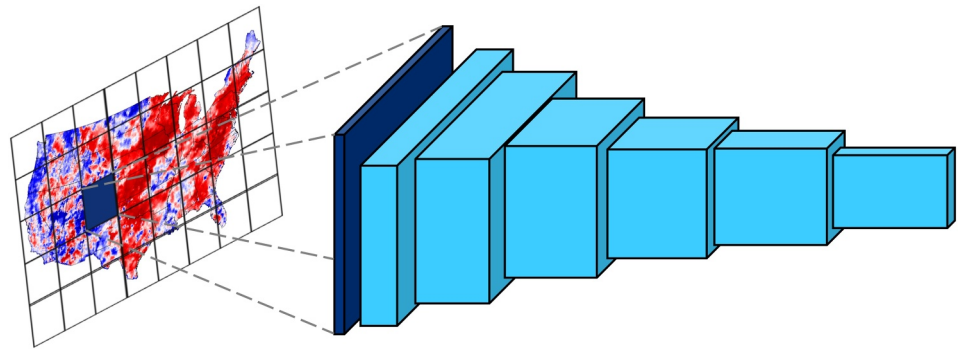

Figure 3. The general architecture of a Markovian discriminator. The dark blue part that is shown to be extracted from the map is a patch (window).

image segment and produce a singular value signifying if the segment is real or synthetic. This approach places additional constraints that promote clear, high-frequency details.

In the architecture of the DroGAN network, a PatchGAN is utilized as the discriminator. The discriminator contains modules in the form of Convolution-BatchNorm-LeakyReLu. All LeakyReLu functions have a slope of 0.2. A convolutional layer is applied after the last layer, followed by a sigmoid activation function to output a one-dimensional image. Figure 3 presents the general architecture of the Markovian discriminator used in DroGAN.

By incorporating PatchGAN, DroGAN is able to generate output maps with improved accuracy in terms of capturing the spatial structure of drought within specific regions. The textual summary of the discriminator model is tabulated in Table S2 in Supporting Information S2.

3.4. Batch Normalization

One of the complications of training DL models is the dynamic distribution of input to each layer, which changes during the training phase. Modifying the parameters of the preceding layer in this process can hinder the training speed since it necessitates using a lower learning rate. To address the issue of internal covariance shift and mitigate the problems related to vanishing gradient descent, batch normalization is employed in both the generator and discriminator blocks of DroGAN (Ioffe & Szegedy, 2015). Internal covariance shift refers to the changing distribution of input to layers in deep networks during the training phase, which can lead to the vanishing gradient descent problem and hinder the training process. The vanishing gradient descent problem becomes significant in deep neural networks as adding more layers can cause the weights to diminish, resulting in computations that yield nearly constant values.

3.5. Activation Function

The activation function plays a crucial role in a neural network by transforming the summed inputs of a neuron into its output. Typically, this function is nonlinear and applies mathematical equations to determine whether the neuron should be activated or not. Additionally, it introduces nonlinearity to the neuron's outputs, enabling more complex representations and behaviors in the network (Vijayakumar et al., 2021). In this study, the LeakyReLU activation function is used in the contracting path of the generator, and ReLU activation function is used in the expansion path, and at the end, the hyperbolic tangent (Tanh) function is used(Varshney & Singh, 2021).

3.6. Loss Function

In DroGAN, we need to define two distinct loss functions for the discriminator and the generator. The objective of the discriminator's loss function is to minimize the negative log-likelihood of correctly identifying observed and simulated SSI maps while considering the SSI observed maps as conditioning information. To achieve this, the Binary Cross Entropy (BCE) loss function is employed in the discriminator (Ho & Wookey, 2020). To identify the optimal loss function for the generator, four different models are constructed, each employing a distinct loss function. In the first model, the loss function solely consists of Mean Absolute Error (MAE). The second model only uses adversarial loss as the loss function. The third model combines the adversarial loss, as provided by the

discriminator, with MAE (*L1*). Lastly, the fourth model incorporates a combination of the adversarial loss and Mean Square Error (MSE) (*L2*) in its loss function.

The adversarial loss assists the generator in determining whether the generated SSI maps resemble the observed maps in terms of their spatial drought structure. Conversely, the *L* loss function guides the generator to produce SSI maps that are pixel-wise consistent with the target domain. The combination of the loss functions is calculated as:

$$\text{Generator loss} = \text{Adverserial loss} + (\lambda \times L) \tag{2}$$

where λ is the hyperparameter that regulates the significance of the L loss relative to the adversarial loss during the training process of the generator.

3.7. DroGAN

As mentioned previously, DroGAN, same as other GANs, contains a generator and a discriminator model. The modified version of the U-Net model is employed to serve as the generator and PatchGAN is used as the discriminator of DroGAN. In each block of the generator and discriminator, the 2D convolutional layers are used to extract the information embedded in the input data to develop the network.

During the network training process, an Adam solver with a learning rate of 10^{-4} was set, and the padding mode was configured as "reflect", a method that adjusts the image size by creating a reflected boundary around the image, aiming to reduce edge effects (Liu et al., 2018). To mitigate the risk of overfitting, three dropout regularization techniques are implemented in the first three layers of the generator's expansion path, employing a dropout rate of 50%.

The U-Net architecture is similar to Figure 2, except that it contains more layers and in the expansion path, the skip connections double the number of channels. The batch size is set to 1, 16, 32, 64, and 128 to study the impacts of batch size on the runtime.

3.8. Accelerating With GPU

DroGAN is coded in a way that takes advantage of both CPU and GPU simultaneously. The datasets are iteratively processed in parallel by multiple CPUs and then transferred to the GPU to train the network. Additionally, Compute Unified Device Architecture (CUDA) is used to optimize the calculations over GPU, which helps improve the training process. CUDA is a novel programming architecture for running computations on GPU, released by NVIDIA (Luebke (2008)). The CUDA toolkit helps to develop and deploy methods on GPU-accelerated systems. In this study, Pytorch in conjunction with CUDA is used to run DroGAN on GPU.

To run DroGAN, we used GPU: NVIDIA A100 80 GB PCIe, installed on the High-Performance Computing (HPC) system in the Center for Complex Hydrosystems Research (CCHR) at The University of Alabama.

3.9. Model Comparison

Inspired by the CNNs, the well-known U-Net, initially conceptualized by Ronneberger et al. (2015) for biomedical imagery segmentation, has shown promising results in climatic studies. These include refining weather forecasts as observed in works by Gronquist et al. (2021) and Hess and Boers (2022), downscaling application as noted in Adewoyin et al. (2021), and precipitation forecasting, as mentioned in Trebing et al. (2021). Additionally, Larraondo et al. (2019) explored multiple encoder-decoder designs and identified U-Net-based structures as optimal for predicting overall rainfall using geopotential height. Meanwhile, Weyn et al. (2020) employed a U-Net design, transforming input grid values into a cubed-sphere. Based on the success of U-Net across varied applications, we trained a U-Net with the same architecture as the generator to compare the results with DroGAN. The inputs to the U-Net model are the same as the inputs to DroGAN. These inputs are divided into training, validation, and testing datasets in the same manner as for DroGAN. The U-Net model is trained on the same GPU, and an early stopping strategy is utilized to mitigate overfitting issues.

As another model, a Naïve approach is implemented, taking the SSI value at time *t-21* to directly represent the prediction. Hence, SSI at time *t* is equated to SSI at time *t-21*.

3.10. Evaluation Metrics

The accuracy evaluation of the modeling is performed using MSE, coefficient of determination (R^2), and Nash-Sutcliffe Efficiency (NSE) coefficient between the simulated and observed SSI maps as follows:

$$MSE = \frac{\sum_{t=1}^{N} (SSI_{pred}^{t} - SSI_{obs}^{t})^2}{N} \tag{3}$$

$$R^2 = \left[\frac{\sum_{t=1}^{N} (SSI_{obs}^{t} - \overline{SSI}_{obs})(SSI_{pred}^{t} - \overline{SSI}_{pred})}{\sqrt{\sum_{t=1}^{N} (SSI_{obs}^{t} - \overline{SSI}_{obs})^2} \sqrt{\sum_{t=1}^{N} (SSI_{pred}^{t} - \overline{SSI}_{pred})^2}} \right]^2 \tag{4}$$

$$NSE = 1 - \frac{\sum_{t=1}^{N} (SSI_{pred}^{t} - SSI_{obs}^{t})^2}{\sum_{t=1}^{N} (SSI_{obs}^{t} - \overline{SSI}_{obs})^2} \tag{5}$$

where SSI_{pred}^{t} and SSI_{obs}^{t} are the model predicted and observed SSI maps in t time step, respectively. $\overline{SSI}_{obs}$ and $\overline{SSI}_{pred}$ are the average map of the model's predicted and observed SSI maps, respectively and N is the total number of the SSI maps.

4. Results and Discussion

The current study develops a GAN for real-time flash drought monitoring based on the SSI index across the CONUS. First, the maps are preprocessed as mentioned in Section 3, and the architecture of DroGAN is designed. In this section, we present the results and discussion of the study.

A key strength of DroGAN is in identifying complex, nonlinear relationships that are the characteristics of the climate systems. Traditional methods, often constrained by predefined equations or assumptions, may over-simplify these relationships. DL models such as DroGAN, however, can autonomously learn from the data, creating models that more accurately reflect the intricate realities of climate change processes. Additionally, the adaptability of DL models is particularly beneficial in the context of climate change. As our planet undergoes continuous environmental shifts, these models can learn and evolve with new data, providing insights that are current and relevant (e.g., training the models using the new datasets that are affected by climate change). This contrasts with traditional models, which may become less accurate or obsolete as environmental conditions change due to the physical relationships that govern the models.

4.1. Loss Function

Choosing an appropriate loss function is an essential aspect when creating a GAN model consisting of two deep learning models operating together in a competitive manner (Elaraby et al., 2022). We compare the performance of the networks with different loss functions to identify the most effective loss function. The evaluation of the models is conducted using R^2, employing a batch size of 64 and 600 epochs. We have set the lambda value for the composite loss functions at 100. The outcomes of this evaluation for the testing phase are presented in Figure 4.

In the comparative analysis of models, we opted to use R^2 as our evaluative metric. This decision is guided by the interpretability of R^2 in quantifying the proportion of the variance in the dependent variable that is predictable from the independent variables.

In our study, we employ both MSE and MAE as the most widely used loss functions in training DL-based models to train DroGAN. This approach is chosen to explore and capture diverse error characteristics: MSE, known for its sensitivity to larger errors, emphasizes error variance, while MAE provides a more balanced focus on the average magnitude of errors. In this study, R^2 is not used as a loss function since it does not provide a directly actionable

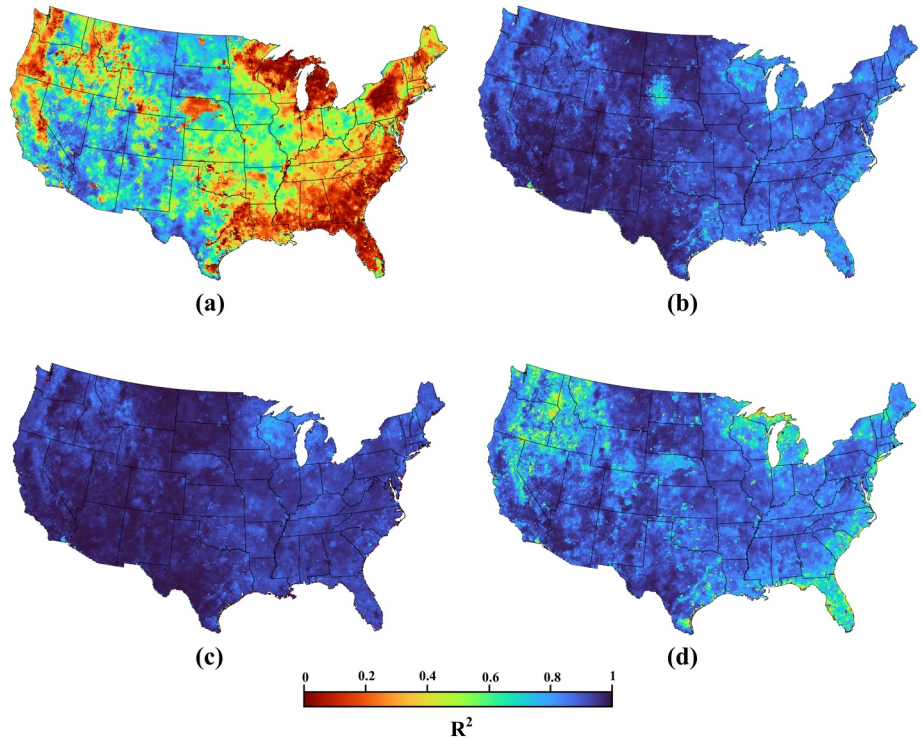

Figure 4. Evaluation results (R^2) of DroGAN using four distinct loss functions, (a) adversarial loss, (b) MAE, (c) combination of adversarial loss and MAE, and (d) combination of adversarial loss and MSE.

gradient for optimization in the same way as MSE or MAE. Particularly in scenarios with non-linear or complex relationships in data, R^2 can be less effective as a training criterion (Nie et al., 2018).

The results of this study (Figure 4) indicate that using the combination of adversarial loss and MAE in DroGAN leads to better performance than the combination of adversarial loss and MSE. In the combination that includes MAE, as the absolute value of an error is calculated, all the errors will be considered on one linear scale. Therefore, the loss function focuses more on how well the model is generally working. Both combined loss functions resulted in better R^2 than utilizing only MAE as the loss function of the generator. These results are in alignment with previous studies that reported using only one of the common loss functions for the generator model leads to blurry output images and using the adversarial loss alone ($\lambda = 0$ in Equation 1) outputs sharper images (Isola et al., 2017). Integrating MAE with adversarial loss (Figure 4c) offers enhanced performance in comparison to employing adversarial loss in isolation (Figure 4a). While the primary objective of the adversarial loss is to calculate the probability that the generated image is a real one, it falls short of guaranteeing pixel-to-pixel similarity with the desired target. Incorporating the *L1* loss (MAE) ensures a pixel-level structural resemblance between the generated and target images.

The above-mentioned loss function is designed that produces a structured loss function and penalizes the difference between the spatial dependencies of output and target maps. In DroGAN, there is no need for hand-engineering the loss function because it is performed inherently in the network as it not only learns to simulate the SSI maps but also learns the loss function in the discriminator section. Combining the *L* error with adversarial loss also promotes the adherence of the GAN model to the input maps; otherwise, the model only aims to synthesize the maps that look realistic, without considering the input maps. Since the loss functions provided by the discriminator model dynamically change with respect to the growth of the generator model, the performance of the generator model improves during the training process. This finding is in agreement with a study stating that training a machine learning model with a dynamic loss function leads to more accurate results (Wu et al., 2018).

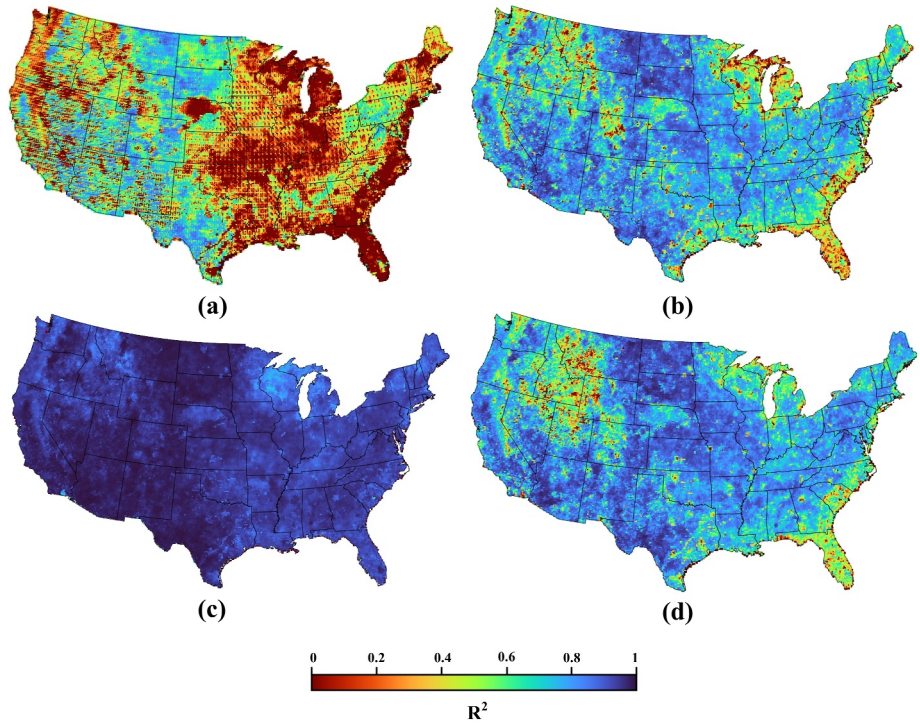

Figure 5. The performance of DroGAN with (a) 10^{-2}, (b) 10^{-3}, (c) 10^{-4}, and (d) 10^{-5} learning rate according to the R^2 metric.

4.2. Optimum Learning Rate

The learning rate determines the magnitude of steps the optimizer takes while adjusting the weights of both the generator and discriminator networks throughout the training process. A higher learning rate might expedite the learning process, but there is a risk that it might lead to a sub-optimal final weight configuration (Zeiler, 2012). In this section, we delve into the effects of varying learning rates on the efficacy of DroGAN in the testing phase, as depicted in Figure 5.

The results (Figure 5) indicate that selecting the learning rate is crucial in training the model as it has a significant impact on the performance of the model. Upon training the model with various learning rates including 10^{-2}, 10^{-3}, 10^{-4}, and 10^{-5}, the distinct patterns in convergence are observed. As shown in Figure 5, training with a high learning rate (e.g., 10^{-2}) leads to erratic R^2 maps, suggesting that the model might be overshooting the minima in the loss landscape. In contrast, an extremely low learning rate (e.g., 10^{-5}) results in a very slow convergence, affecting the computational efficiency. Here, we trained the model with a 10^{-5} learning rate for 2,000 epochs; however, the performance of the model is not as efficient as when the model is trained with a 10^{-4} learning rate for 600 epochs.

4.3. Determining the Optimum Epoch Number

The inherent complexity of the dataset is the main factor in determining the optimum number of epochs, which is the number of times the learning algorithm performs on the training dataset. The overfitting problem is a significant issue in training a DL model. One of the causes for this problem is setting the wrong number of epochs in the training phase. To determine the optimum epoch number, the performance of the network is evaluated using the R^2 metric in different epochs from 10 to 1,000 over the validation set. Figure 6 presents the R^2 results for different epoch numbers in the validation phase.

The results indicate that 600 is the optimum epoch number to train the DroGAN model. According to the results (Figure 6), starting from 400 epochs, the performance of the model becomes stable and some improvements in R^2 are seen up to 600. Training the model with less than 400 epochs leads to an abundant amount of noise in the simulated SSI maps. When the epoch number is increased from 600 to 1,000, it potentially results in a decline in

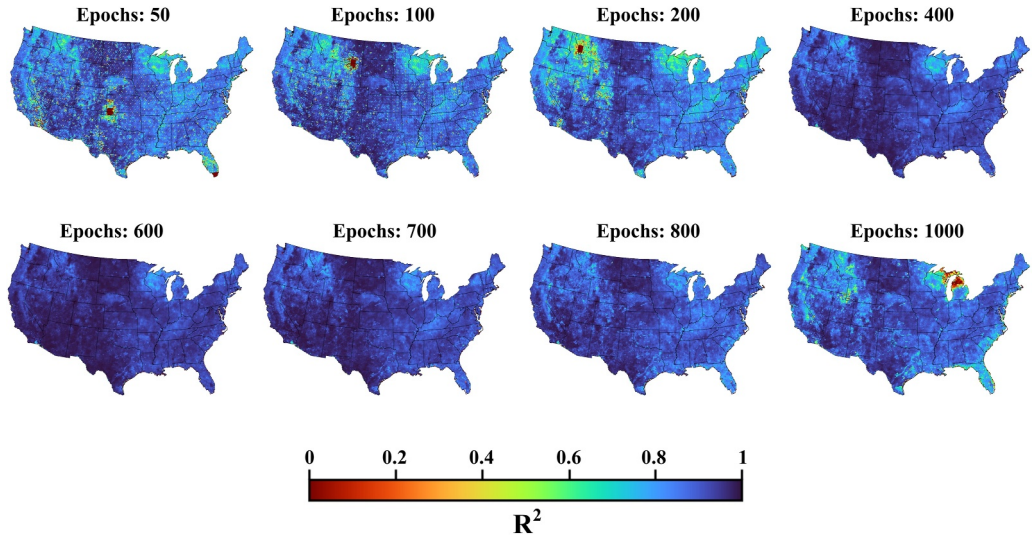

Figure 6. The performance of DroGAN in different epoch numbers according to the R^2 metric. The results show that the performance of the network increased up to 600 epochs and after that, the network encountered an overfitting problem.

the network's performance. This decrease in performance may indicate the presence of an overtraining problem. In most of the studies, GANs need a large epoch number (>100) to reach the best performance (Bird et al., 2022; Robic-Butez & Win, 2019; Sarp, Kuzlu, Pipattanasomporn, & Guler, 2021; Sarp, Kuzlu, Wilson, & Guler, 2021); while there are a few studies that reported lower epoch numbers to train their proposed GAN or use an already existing GAN for an application (Laloy et al., 2018; Li et al., 2020). Generally, there is no universal agreement on the optimal epoch number for training a GAN network. The number depends on the type, size, and application.

4.4. Optimum Batch Size on GPU

To determine the optimum batch size and compare the execution times, multiple iterations of DroGAN are conducted using different batch sizes and a maximum of 600 epochs. The batch size refers to the number of training samples processed before modifying the model's internal parameters. After each epoch in each setup, the timing data is recorded, and the cumulative results are displayed in Figure S1 in Supporting Information S1.

The initial epoch in each configuration takes longer to run compared to subsequent epochs. The variation in timing between the first epoch and subsequent epochs can be attributed to the generation and loading of data into memory, which occurs at the beginning of the first epoch. Furthermore, during the coding process, the CUDA auto-tuner is activated to evaluate different algorithm variations in the first epoch. This selection process identifies the fastest algorithm for the specific configuration and utilizes it to train the model in the subsequent epochs. While this initialization process takes more time in the first epoch, it optimizes the training procedure in the following epochs and reduces the overall cumulative training time consumption.

The results (Figure S1 in Supporting Information S1) indicate that increasing the batch size to a larger number (up to 64) helps to decrease the run time due to the multi-threading and matrix multiplication abilities of GPUs. The optimum batch size in this study for training DroGAN on the GPU is 64. Increasing the batch size from 64 to 128 increases the run time which is due to the finite capabilities of the GPU.

4.5. Model Performance

The performance of DroGAN is evaluated using the performance measures discussed in Section 3.10, including R^2, NSE, and MSE, the results of which are presented in Figure 7 for the testing phase. The results suggest that the model effectively estimates SSI in various regions of CONUS. However, the degraded model performance is seen in the upper Midwest, Mideastern, Northeastern, and Western states of CONUS (shown by gray rectangles in Figure 7a). These states, characterized by mountainous terrain and high snowfall, exhibit lower performance for DroGAN. This observation aligns with previous research findings, where several studies have also reported

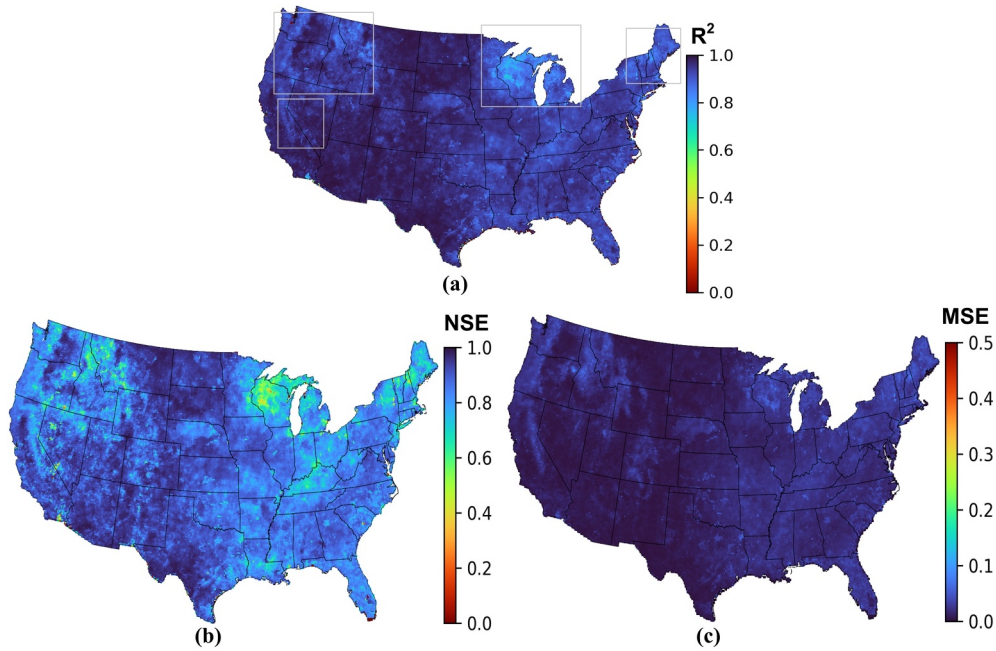

Figure 7. The evaluation results of DroGAN using (a) R^2, (b) NSE, and (c) MSE.

decreased model performance in snow-dominant and mountainous regions (e.g., Cai et al., 2014; Markstrom et al., 2016; Mazrooei & Sankarasubramanian, 2019; Wrzesien et al., 2019).

The diminished performance of DroGAN in mountainous and snow-dominant regions may stem from a scarcity of data representative of these areas. Given the limited geographical spread of such climates compared to others, the available datasets may not sufficiently capture the unique environmental dynamics present. In mountainous regions, the interaction between hydrological processes and snow cover bears significant importance, similar to other snow-dominant areas. Temperature plays a crucial role in influencing streamflow in these snow-rich environments. Furthermore, the interaction of temperature with elevation can lead to varying effects on drought onset, particularly due to the presence of snow. Soil characteristics are another vital aspect, influencing infiltration, water capacity, and rooting depth, which in turn, affect subsurface water flow, discharge rates, and soil moisture in mountain regions (Bennie et al., 2008; Moeslund et al., 2013; Strachan & Daly, 2017). Baseflow, shaped by region-specific natural factors, also exerts a direct and indirect influence on drought dynamics in these areas (Konapala & Mishra, 2020). The slow movement of groundwater in mountainous areas results in extended baseflow periods, subsequently impacting soil moisture. Moreover, certain climatic variables that significantly influence soil moisture and agricultural drought in other regions may manifest differently in mountainous landscapes. For instance, the limited time for rainfall storage at higher altitudes impacts the primary sources of soil moisture in these regions. There are notable disparities in NSE values across different snow-dominant regions. For example, DroGAN exhibits lower performance in Northern Michigan compared to areas like California's Sierra Nevada. This variability is likely due to differences in snow density and water content, which are shaped by regional temperature, precipitation types, and other climatic factors, thus influencing soil moisture dynamics. Consequently, the model struggles to accurately capture these dynamics in certain regions compared to others. The primary reason for this reduced efficacy may be the limitations within the training dataset, particularly in representing conditions prevalent in snow-dominated regions. Inadequate representation of data from similar climatic areas in the training set can hinder the model's ability to generalize effectively to such environments.

NLDAS-2 could also contribute to the model's suboptimal performance in certain areas. Data provided by NLDAS-1 in mountainous regions tends to have a significant negative bias (Pan et al., 2003). To mitigate this bias in NLDAS-2, parameter-elevation regressions are incorporated into the Independent Slopes Model climatology, which helps reduce the negative bias. However, the precipitation data has not yet been bias-corrected, leading to biases in the evapotranspiration (ET) simulations (Xia et al., 2015). Furthermore, studies have shown that the ET product of NLDAS exhibits poor accuracy when compared to observation data in forested regions (Xia

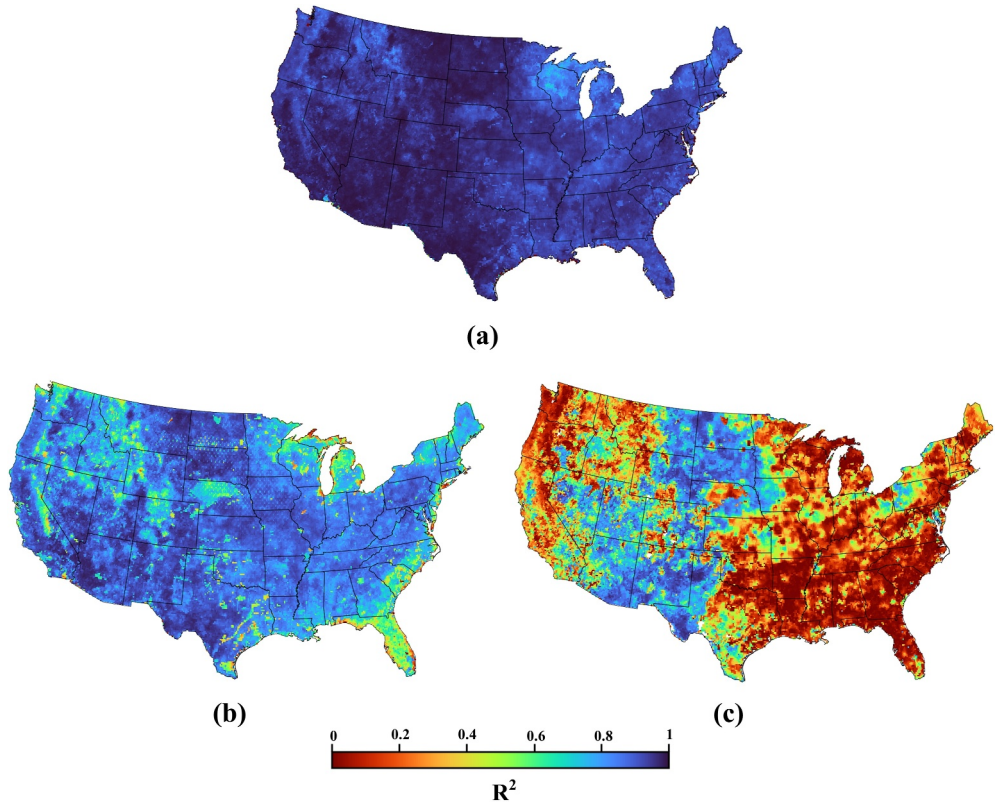

Figure 8. Evaluation results based on R^2 of (a) DroGAN, (b) U-Net, and (c) Naïve models.

et al., 2012, 2014). The presence of biased input data in mountainous and forested areas could be one of the reasons for the lower performance of DroGAN in these regions. It is crucial to address the bias in the input data because it is likely that the model retains this biased information during the training process, as highlighted by Kim et al., in 2019.

This reduced performance could also be attributed to the use of MAE in the loss function, as it introduces blurriness to the synthesized image when the model is uncertain about the exact location of an edge.

4.6. Comparative Performance Analysis

In this section, we compare the performance of our proposed model, DroGAN, against the U-Net architecture and a Naïve model for predicting SSI. The hyperparameter tuning results for the U-Net model is provided in Figures S2–S3 in Supporting Information S1. The U-Net model is trained with the MSE loss function and learning rate 10^{-4}. The comparison of the models is conducted using R^2 and the outcomes of this evaluation are presented in Figure 8 for the testing phase.

In our comparative analysis, we observe that the DroGAN model outperformed the U-Net model in predicting SSI. While both models have performed considerably better than the Naïve model, the specific nuances of SSI prediction seem to be more amenable to the structure and mechanics of the DroGAN model. Table S3 in Supporting Information S2 presents the training phase run times for both DroGAN and U-Net using the same computational resources. Although U-Net's training is faster than DroGAN, it results in lower accuracy. Our comparative study between the DroGAN and U-Net models (Figure 8) demonstrates that while DroGAN requires a longer training duration, this investment is justified by its superior accuracy and robustness. The DroGAN model excels in capturing complex patterns in data, which results in enhanced performance metrics. Furthermore, the adversarial training mechanism of DroGAN contributes to higher accuracy and its generalization capabilities. One possible explanation for DroGAN's enhanced performance is its adaptive loss function, which adjusts according to the network's performance. This function optimizes the network to have a better performance during both training and testing phases. While U-Net is undoubtedly a powerful architecture, DroGAN, by integrating

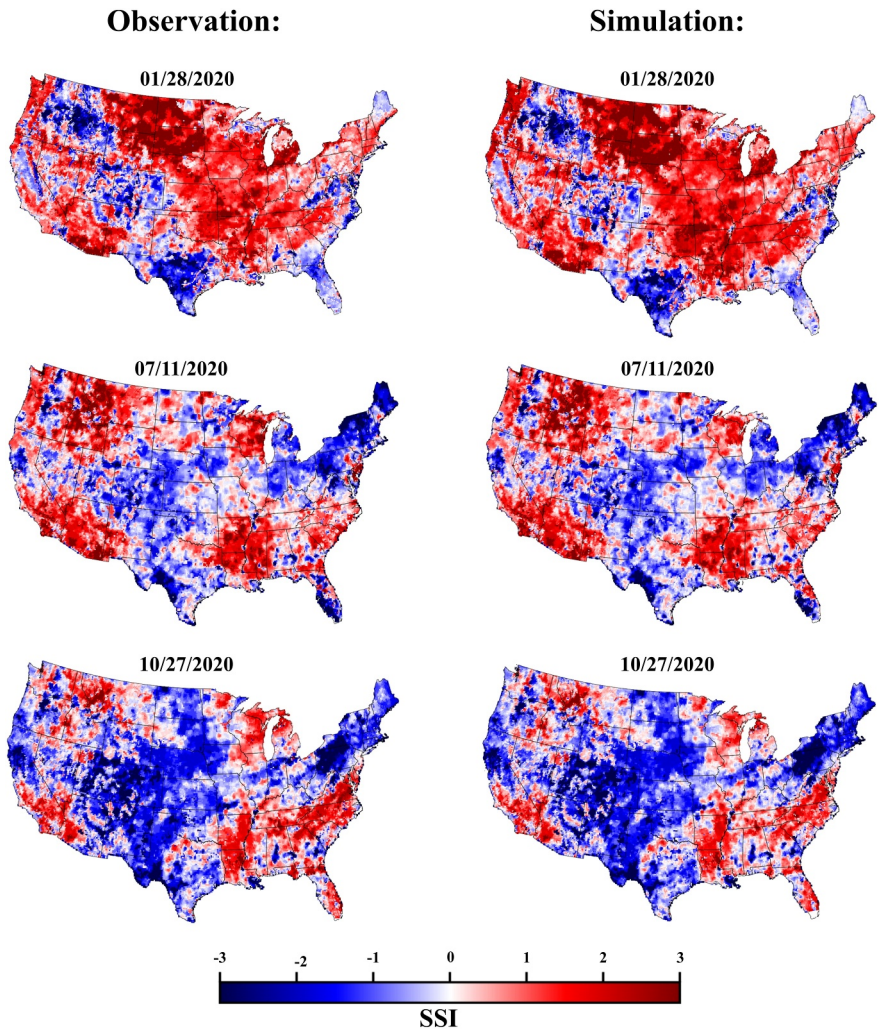

Figure 9. The outputs of DroGAN and target images on randomly selected days. Comparing the maps indicates that the network successfully estimates SSI.

the U-Net model with a discriminator, shows to be more adept at capturing both local and global features. Furthermore, the adversarial loss encourages the network to account for spatial dependencies between neighboring regions during the modeling stage. Additionally, the adversarial training approach used by DroGAN ensures the model is optimized such that its generated maps (predictions) closely mirror observed SSI maps and increases the generalizability of the model.

4.7. Examples of Spatial and Temporal Distribution

The simulated SSI maps for random days are compared to the observed SSI maps across the CONUS in Figure 9. In addition, the outputs of the network are categorized into drought intensity maps using Table 1 and compared with the relevant drought intensity maps provided by USDM over the CONUS in Figure 10.

The results presented in Figure 9 demonstrate that the simulations align with the observed maps, indicating that the network is capable of capturing the patterns and values of SSI. Overall, the network successfully replicates the large-scale patterns observed in SSI. However, Figure 9 exemplifies that the SSI values in the upper Midwest, Midwestern, Northeastern, and Western states of CONUS exhibit somewhat erratic spatial patterns, which can explain the lower accuracy of DroGAN in these regions. On the other hand, the network effectively captures the detailed patterns of SSI spatial distribution in other areas. Nevertheless, in a few regions such as the Northeastern, Southeastern, and east-central regions, the network tends to display a white color (SSI = 0), indicating

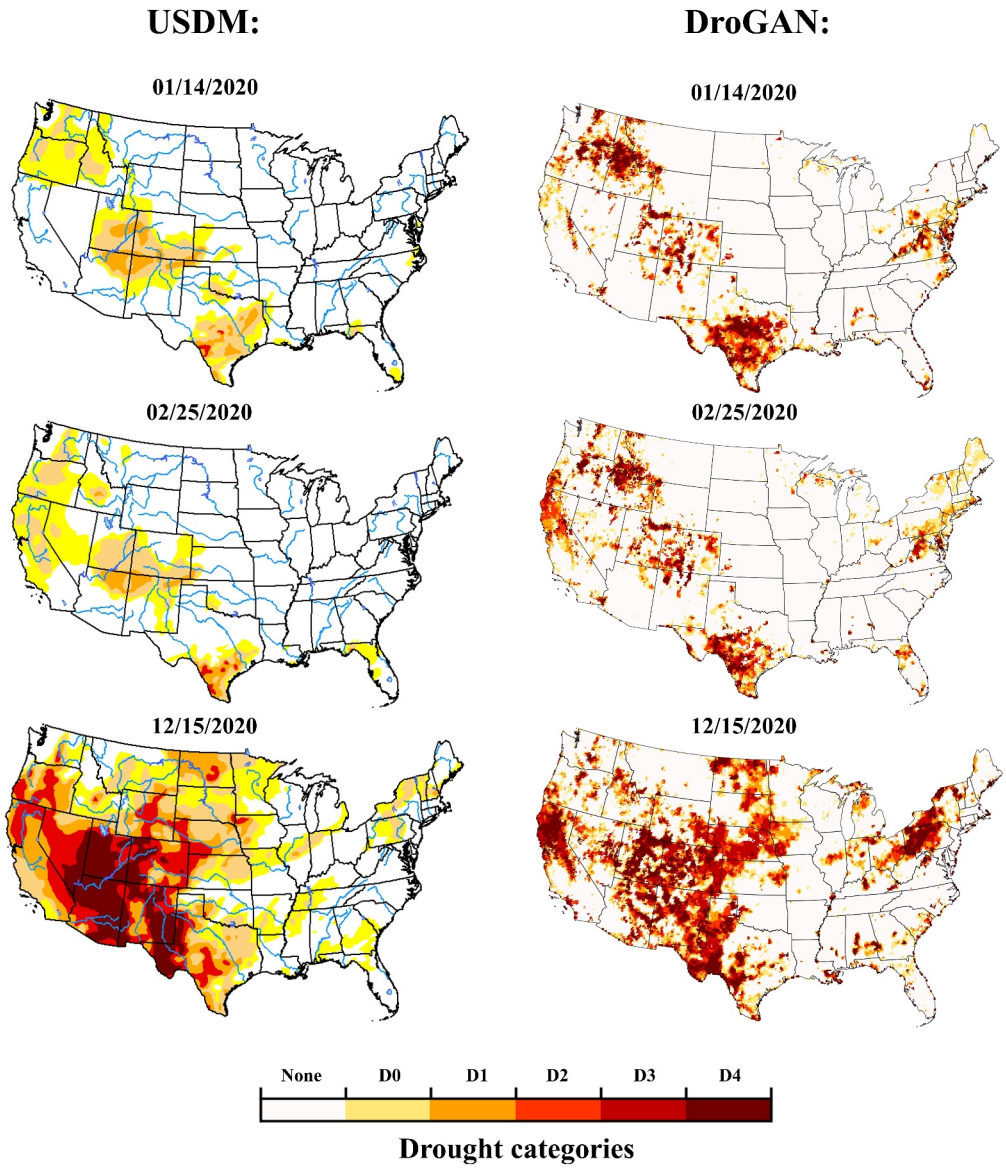

Figure 10. Comparison of USDM drought maps and flash drought maps obtained by DroGAN over the CONUS for three randomly selected days.

non-drought conditions. This behavior may be related to the MAE component of the loss function, which encourages an average value (in this case, 0) when the model is unsure about the appropriate SSI value for a specific pixel (Cheng et al., 2022).

Investigating Figure 10, the random drought maps from the testing dataset illustrate the success of DroGAN in flash drought monitoring. In general, the network effectively captured both general drought patterns across almost all regions. Although both the USDM and DroGAN drought maps are categorized based on Table 1, there are some differences between the provided maps. For instance, according to the USDM drought map on 14 January 2020, the D0, and D1 drought conditions were observed in the northwestern, west-central, and south-central regions, and only a small area in Texas experienced drought with category D3. However, the DroGAN map indicates that the majority of these regions experienced D2 and D3 drought conditions, and some regions were in category D4. Similarly, on 25 February 2020, the DroGAN drought map displayed D0, D1, and D2 drought conditions in the northwestern areas, whereas the USDM map indicates D0 and D1 conditions in these regions. Another example can be explained for 15 December 2020, where the USDM characterized D0 and D1

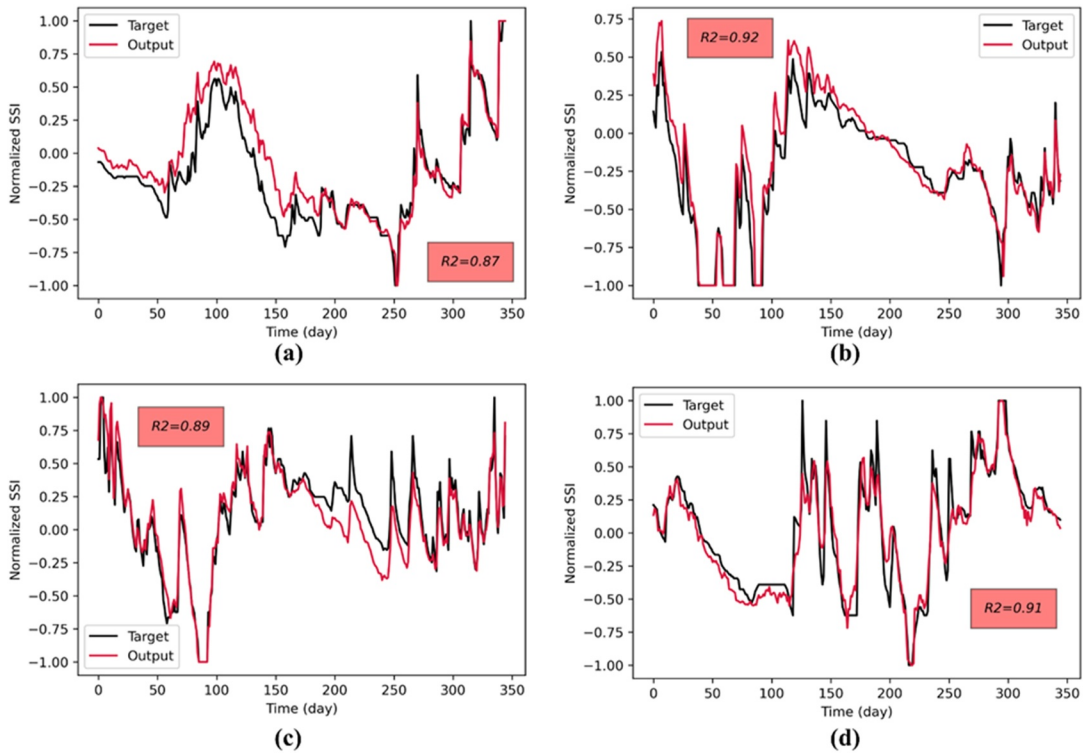

Figure 11. The simulated and observed time series in 2020 for SSI in (a) New York, (b) Nevada, (c) Montana, and (d) Alabama states.

drought conditions in the northeastern CONUS, while DroGAN shows a wider range of drought conditions, including D0–D4, in these areas. The primary reason for these discrepancies between the maps may be that the USDM maps consider various variables, including groundwater data, for mapping drought. In contrast, DroGAN's simulations are solely based on SSI maps, and the model generates drought maps exclusively using soil moisture information.

One of the main proposed approaches to investigate flash drought is studying soil moisture variations because they are important drivers of vegetation stress during drought situations particularly when soil moisture reaches the wilting point. Plants respond to soil moisture conditions by regulating their water consumption and balancing evaporative demand with the availability of moisture. Therefore, soil moisture is an important indicator of early vegetation drought stress. It has been shown that soil moisture rapidly decreases during the early stages of a flash drought due to increasing ET (Ford & Labosier, 2017).

Due to the escalating effects of climate change and human activities, the need for drought risk management policies has increased, necessitating the examination of spatial and temporal drought patterns in various regions (J. Li et al., 2021; P. Li et al., 2021). Moreover, it is essential to analyze the patterns of SSI time series to assess the efficacy of using DroGAN for studying flash droughts, which are characterized by rapid intensification within a short period. To address this, DroGAN was employed to estimate daily SSI maps across the CONUS in 2020. Subsequently, specific locations were randomly selected in different regions, and the corresponding time series were plotted to evaluate the model's performance. The outcomes of this analysis are depicted in Figure 11.

The results (Figure 11) indicate that the model effectively captured the temporal patterns of SSI in various locations. Overall, the model demonstrates excellent performance, with coefficient of determination ($R^2 \geq 0.85$) in the time series, reproducing the temporal patterns of SSI. However, there are instances of lower model performance observed in New York and Montana states, corresponding to points located in the northeastern and western regions of the CONUS. The reasons for this reduced performance in these regions were previously discussed in the preceding sections. According to Figure 11, the model proves to be reliable for studying flash droughts, as it effectively captures sudden changes in SSI temporal patterns in different locations.

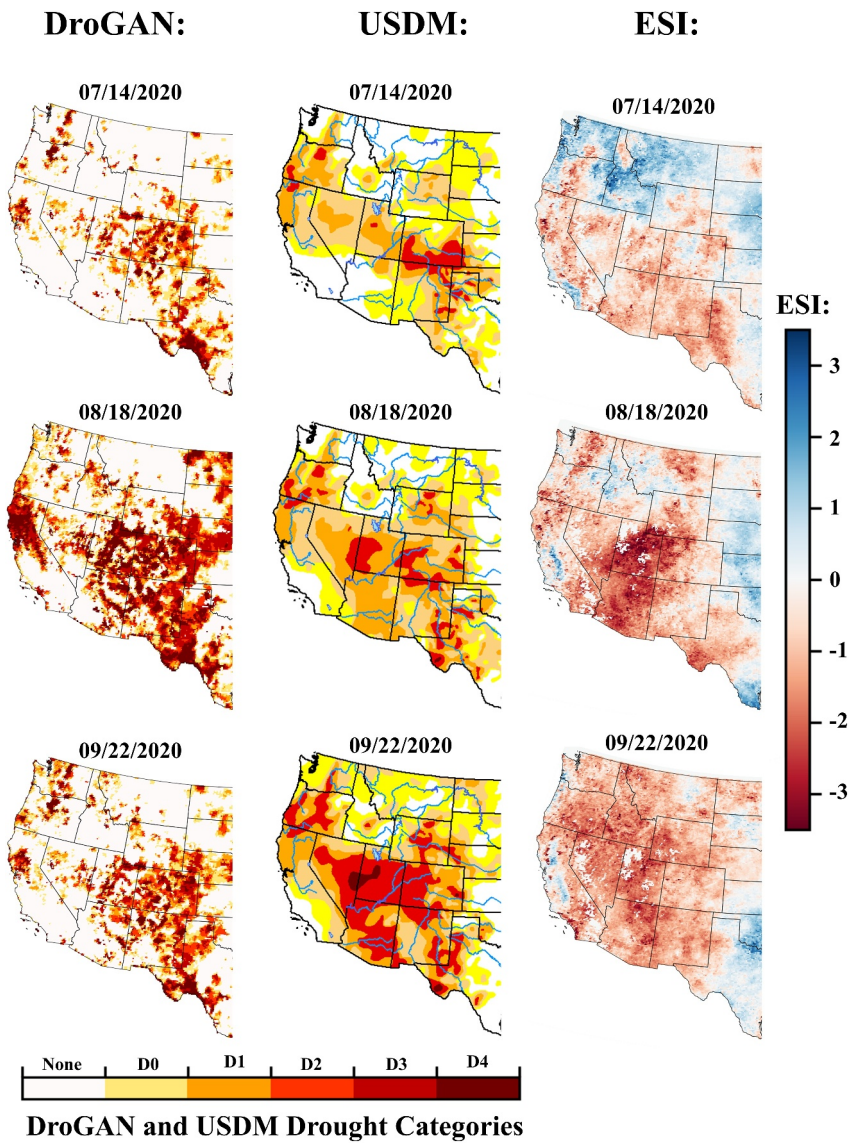

Figure 12. Comparison of DroGAN, USDM, and ESI drought maps for July-September 2020 for a reported flash drought in the western U.S.

4.8. Evolution of 2020 Flash Drought in the CONUS

Since the early 2000s, extensive portions of the western U.S. have suffered a prolonged "megadrought", influenced by both natural climate conditions and human activity (Williams et al., 2020). A temporary improvement occurred in 2019, but the drought worsened again in the mid-2020s due to a La Niña event, which led to reduced rainfall and extended heatwaves (Sehgal et al., 2021). To assess the effectiveness of DroGAN in generating the drought maps, we compared DroGAN-generated drought maps with that of the USDM and the flash drought detection by ESI. Previously, the ESI maps were demonstrated to provide reliable assessments of flash drought evolution (Anderson et al., 2016; Otkin et al., 2013). This section demonstrates how well DroGAN-generated drought maps perform in an actual flash drought situation.

The temporal evolution of drought severity in the western U.S. during July–September 2020 (Figure 12) reveals a strong spatial correlation between ESI and SSI (DroGAN outputs) indices. Drought maps based on ESI and SSI methods reveal an escalation of drought conditions in August 2020 across several states including Utah, western Colorado, southern Nevada, western Texas, Arizona, and New Mexico. These indices indicate a temporary decline in drought levels by late September 2020, which can be attributed to winter rainfall in the central plains

(NOAA/NIDIS, 2021). While the USDM drought maps are generally in line with other drought maps, they seem to be less effective in identifying the onset of flash droughts in August. Moreover, because USDM maps consider a variety of factors, the winter rainfall does not result in a reduction of drought levels according to these maps.

The USDM drought maps are provided based on multivariable inputs which is a robust aspect of these maps for prolonged drought monitoring. However, the validation of the drought maps provided by USDM for flash drought identification has shown that the maps can successfully determine the spatial extent of a developed flash drought event, while it contains lags in showing the rapid onset. The delay in capturing the flash drought features and intensities is related to the multivariable characteristics of the USDM drought maps (Otkin et al., 2013, 2018). While the ESI maps are suitable for flash drought monitoring, they are provided on a weekly basis. However, DroGAN is able to provide daily SSI maps for flash drought monitoring.

5. Summary and Conclusion

Flash drought monitoring holds significant importance in various domains, particularly in agricultural and water resources management. Recent studies have identified numerous regions that have witnessed occurrences of flash droughts in recent years. Consequently, the current study focuses on the development of a deep learning model for real-time flash drought monitoring using remotely sensed images. The study utilizes daily data on ET, SM, T, and LAI from the NLDAS-2 dataset, and daily SSI maps from a new collection spanning the CONUS between 2016 and 2020. While the current model utilizes the exogenous variables at time t for predicting SSI, an interesting avenue for future research would be to explore the potential benefits of incorporating the temporal evolution of these variables into the model. Furthermore, incorporating additional input variables such as snow water equivalent (SWE) into the model could enhance its performance in snow-dominant regions or mountainous areas. Additionally, considering the uncertainty of each variable in predicting the flash drought indices can be a new avenue of research. Over 9,000 images (including 7,312 input images and 1,828 target images) are preprocessed, normalized, and transformed into appropriate tensors for use as input and target images in the model. Several configurations are executed to determine the optimal number of epochs for the model, with the results indicating that 600 epochs yield the best performance. It is concluded that there is no universal guideline for determining the optimal epoch number in a GAN model, as it is highly dependent on the dataset. Furthermore, different configurations of DroGAN are tested to identify the optimal batch size, considering both CPU and GPU computations. Additionally, running the model on GPU and leveraging CUDA optimization significantly reduces the execution time compared to using CPU alone $\left(\frac{Run\ time\ (CPU)}{Run\ time\ (GPU\ and\ CUDA)} = 696\right)$. It is worth mentioning that the GAN-based models are highly sensitive to the values of hyperparameters and training a GAN model is challenging due to the minmax game between the networks. Therefore, for each study, a separate GAN model should be optimized.

The developed GAN has some significant advantages compared to conventional DL models. These advantages include an adaptive loss function and the ability of the network to detect spatial patterns and dependencies of drought in different regions. The generator model of DroGAN utilizes a modified version of U-Net, and a PatchGAN to model SSI maps. After the original U-Net was proposed, several advancements have been made, including but not limited to U-Next and Res-UNet. Incorporating the upgraded U-Nets as the generator of DroGAN may improve the accuracy of the model in future studies. The output of the discriminator, referred to as adversarial loss, is integrated into the generator's loss function to design a loss function for the generator. Comparing the DroGAN model's efficacy with that of the U-Net and Naïve models indicates that DroGAN was a more robust architecture.

Selecting an appropriate loss function is a crucial aspect when developing a GAN model. In this research, the BCE loss function is employed for the discriminator, while a hybrid loss function comprising adversarial loss, MSE, and MAE is devised for the generator. The findings demonstrate that integrating adversarial loss with MAE yields more precise and accurate maps compared to solely employing MAE or only adversarial loss or combining adversarial loss with MSE. While we account for several key factors influencing the performance of DroGAN, we rely on prior studies for certain factors and hyperparameters, including lambda (for the combined loss function). Exploring these aspects further in future research could enhance the model's performance. The evaluation of DroGAN's performance in modeling SSI reveals that the model network is generally accurate in most areas. However, it exhibits lower performance in mountainous regions and areas with snow cover. This can be attributed

to the distinct hydrological characteristics of mountainous and snow-dominant areas, which pose challenges for the model. Another contributing factor is the biased input data provided by NLDAS in these regions. To address this issue, it is recommended to employ alternative remote sensing datasets in future studies to assess the model's performance and investigate the impact of input images on the network. Furthermore, the utilization of blur induction and incentivizing averaged values through MAE in the loss function for regions with chaotic changes can also contribute to the problem. Therefore, the development of new loss functions is suggested to prevent such issues in future projects, thereby enhancing the applicability of GAN models in hydrology and water resources.

Additionally, a comparison between the DroGAN drought maps and the USDM agricultural drought maps reveals some discrepancies. This could be attributed to the fact that the USDM drought maps are generated by considering multiple variables such as groundwater and soil moisture, whereas DroGAN outputs only SSI maps, which have shown greater accuracy in studying the onset of flash droughts. In order to assess the performance of DroGAN in detecting flash droughts, the SSI time series for random points in the CONUS are plotted, and the results demonstrate that the network is reliable in capturing sudden changes in SSI temporal patterns, thus making it suitable for flash drought detection. The SSI is determined based on a 30-year data span, and its values may vary depending on the specific 30-year period under consideration; therefore, different 30-year periods may yield varied SSI values (Yuan et al., 2023). It is recommended that future studies delve deeper into this issue and utilize models to forecast other flash drought indicators or soil moisture values.

Every year, droughts have significant financial consequences for both human activities and the environment worldwide, amounting to millions of dollars. Consequently, the creation of innovative models and techniques to monitor droughts in real time is essential for various decision-makers, such as water resource and agricultural managers. Nowadays, progress in image processing and deep learning methodologies, along with the development of novel approaches to training more complex models at a lower computational cost and in less time, aid researchers in achieving greater accuracy during the modeling process.

Data Availability Statement

The NLDAS dataset used in this study was downloaded from NASA's website (https://ldas.gsfc.nasa.gov/nldas/nldas-2-model-data). The SSI maps and the codes are available in the following repository (https://github.com/hmoradkhani/DroGAN/tree/main).

Acknowledgments
The authors acknowledge the financial support provided by the National Science Foundation (NSF-INFEWS) (Grant EAR-1856054).

References

Adewoyin, R. A., Dueben, P., Watson, P., He, Y., & Dutta, R. (2021). TRU-NET: A deep learning approach to high resolution prediction of rainfall. *Machine Learning*, *110*(8), 2035–2062. https://doi.org/10.1007/s10994-021-06022-6

Ahmadalipour, A., & Moradkhani, H. (2017). Analyzing the uncertainty of ensemble-based gridded observations in land surface simulations and drought assessment. *Journal of Hydrology*, *555*, 557–568. https://doi.org/10.1016/j.jhydrol.2017.10.059

Ahmadalipour, A., Moradkhani, H., Yan, H., & Zarekarizi, M. (2017). Remote Sensing of Drought: Vegetation, Soil Moisture, and Data Assimilation. In Lakshmi, V. (ed) *Remote Sensing of Hydrological Extremes. Springer Remote Sensing/Photogrammetry*. Springer. https://doi.org/10.1007/978-3-319-43744-6_7

Anderson, M. C., Zolin, C. A., Sentelhas, P. C., Hain, C. R., Semmens, K., Yilmaz, M. T., et al. (2016). The Evaporative Stress Index as an indicator of agricultural drought in Brazil: An assessment based on crop yield impacts. *Remote Sensing of Environment*, *174*, 82–99. https://doi.org/10.1016/j.rse.2015.11.034

Antipov, G., Baccouche, M., & Dugelay, J.-L. (2017). *Face aging with conditional generative adversarial networks* (pp. 2089–2093). 2017 IEEE International Conference on Image Processing (ICIP). https://doi.org/10.1109/ICIP.2017.8296650

Bennie, J., Huntley, B., Wiltshire, A., Hill, M. O., & Baxter, R. (2008). Slope, aspect and climate: Spatially explicit and implicit models of topographic microclimate in chalk grassland. *Ecological Modelling*, *216*(1), 47–59. https://doi.org/10.1016/j.ecolmodel.2008.04.010

Bird, J. J., Barnes, C. M., Manso, L. J., Ekárt, A., & Faria, D. R. (2022). Fruit quality and defect image classification with conditional GAN data augmentation. *Scientia Horticulturae*, *293*, 110684. https://doi.org/10.1016/j.scienta.2021.110684

Cai, X., Yang, Z. L., Xia, Y., Huang, M., Wei, H., Leung, L. R., & Ek, M. B. (2014). Assessment of simulated water balance from Noah, Noah-MP, CLM, and VIC over CONUS using the NLDAS test bed. *Journal of Geophysical Research*, *119*(22), 13751–13771. https://doi.org/10.1002/2014JD022113

Chen, L. G., Gottschalck, J., Hartman, A., Miskus, D., Tinker, R., & Artusa, A. (2019). Flash drought characteristics based on US drought monitor. *Atmosphere*, *10*(9), 498. https://doi.org/10.3390/atmos10090498

Chen, Q., Cui, Z., Liu, G., Yang, Z., & Ma, X. (2022). Deep convolutional generative adversarial networks for modeling complex hydrological structures in Monte-Carlo simulation. *Journal of Hydrology*, *610*, 127970. https://doi.org/10.1016/j.jhydrol.2022.127970

Cheng, H. Y., Yu, C. C., & Li, C. Y. (2022). Improved two-stage image inpainting with perceptual color loss and modified region normalization. *Machine Vision and Applications*, *33*(6), 94. https://doi.org/10.1007/s00138-022-01344-4

Christian, J. I., Basara, J. B., Otkin, J. A., & Hunt, E. D. (2019). Regional characteristics of flash droughts across the United States. *Environmental Research Communications*, *1*(12), 125004. https://doi.org/10.1088/2515-7620/ab50ca

Christian, J. I., Basara, J. B., Otkin, J. A., Hunt, E. D., Wakefield, R. A., Flanagan, P. X., & Xiao, X. (2019). A methodology for flash drought identification: Application of flash drought frequency across the United States. *Journal of Hydrometeorology*, *20*(5), 833–846. https://doi.org/10.1175/JHM-D-18-0198.1

De Lannoy, G. J., Bechtold, M., Albergel, C., Brocca, L., Calvet, J. C., Carrassi, A., et al. (2022). Perspective on satellite-based land data assimilation to estimate water cycle components in an era of advanced data availability and model sophistication. *Frontiers in Water*, *4*, 981745. https://doi.org/10.3389/frwa.2022.981745

Edris, S. G., Basara, J. B., Christian, J. I., Hunt, E. D., Otkin, J. A., Salesky, S. T., & Illston, B. G. (2023). Analysis of the critical components of flash drought using the standardized evaporative stress ratio. *Agricultural and Forest Meteorology*, *330*, 109288. https://doi.org/10.1016/j.agrformet.2022.109288

Elaraby, N., Barakat, S., & Rezk, A. (2022). A conditional GAN-based approach for enhancing transfer learning performance in few-shot HCR tasks. *Scientific Reports*, *12*(1), 16271. https://doi.org/10.1038/s41598-022-20654-1

Ford, T. W., & Labosier, C. F. (2017). Meteorological conditions associated with the onset of flash drought in the Eastern United States. *Agricultural and Forest Meteorology*, *247*, 414–423. https://doi.org/10.1016/j.agrformet.2017.08.031

Foroumandi, E., Nourani, V., Dąbrowska, D., & Kantoush, S. A. (2022). Linking spatial–temporal changes of vegetation cover with hydro-climatological variables in terrestrial environments with a focus on the lake Urmia Basin. *Land*, *11*(1), 115. https://doi.org/10.3390/land11010115

Foroumandi, E., Nourani, V., Jeanne Huang, J., & Moradkhani, H. (2023). Drought monitoring by downscaling GRACE-derived terrestrial water storage anomalies: A deep learning approach. *Journal of Hydrology*, *616*, 128838. https://doi.org/10.1016/j.jhydrol.2022.128838

Foroumandi, E., Nourani, V., & Kantoush, S. A. (2022). Investigating the main reasons for the tragedy of large saline lakes: Drought, climate change, or anthropogenic activities? A call to action. *Journal of Arid Environments*, *196*, 104652. https://doi.org/10.1016/j.jaridenv.2021.104652

Foroumandi, E., Nourani, V., & Sharghi, E. (2021). Climate change or regional human impacts? Remote sensing tools, artificial neural networks, and wavelet approaches aim to solve the problem. *Hydrology Research*, *52*(1), 176–195. https://doi.org/10.2166/nh.2020.112

Gavahi, K., Abbaszadeh, P., & Moradkhani, H. (2022). How does precipitation data influence the land surface data assimilation for drought monitoring? *Science of the Total Environment*, *831*, 154916. https://doi.org/10.1016/j.scitotenv.2022.154916

Gavahi, K., Abbaszadeh, P., Moradkhani, H., Zhan, X., & Hain, C. (2020). Multivariate assimilation of remotely sensed soil moisture and evapotranspiration for drought monitoring. *Journal of Hydrometeorology*, *21*(10), 2293–2308. https://doi.org/10.1175/JHM-D-20-0057.1

Goodfellow, I., Pouget-Abadie, J., Mirza, M., Xu, B., Warde-Farley, D., Ozair, S., & Bengio, Y. (2014). Generative adversarial nets. *Advances in Neural Information Processing Systems*, *27*.

Grönquist, P., Yao, C., Ben-Nun, T., Dryden, N., Dueben, P., Li, S., & Hoefler, T. (2021). Deep learning for post-processing ensemble weather forecasts. *Philosophical Transactions of the Royal Society A*, *379*(2194), 20200092. https://doi.org/10.1098/rsta.2020.0092

Hammond, J. C., Simeone, C., Hecht, J. S., Hodgkins, G. A., Lombard, M., McCabe, G., et al. (2022). Going beyond low flows: Streamflow drought deficit and duration Illuminate distinct spatiotemporal drought patterns and trends in the U.S. During the last Century. *Water Resources Research*, *58*(9). https://doi.org/10.1029/2022wr031930

Hastie, T., Tibshirani, R., & Tibshirani, R. (2020). Best subset, forward stepwise or Lasso? Analysis and recommendations based on extensive comparisons. *Statistical Science*, *35*(4), 579–592. https://doi.org/10.1214/19-STS733

Hess, P., & Boers, N. (2022). Deep learning for improving numerical weather prediction of heavy rainfall. *Journal of Advances in Modeling Earth Systems*, *14*(3), e2021MS002765. https://doi.org/10.1029/2021MS002765

Ho, Y., & Wookey, S. (2020). The real-world-weight cross-entropy loss function: Modeling the costs of mislabeling. *IEEE Access*, *8*, 4806–4813. https://doi.org/10.1109/ACCESS.2019.2962617

Ioffe, S., & Szegedy, C. (2015). Batch normalization: Accelerating deep network training by reducing internal covariate shift. *International Conference on Machine Learning*, 448–456.

Iqbal, H. (2018). Harisiqbal88/plotneuralnet v1. 0.0. *Zenodo*. https://doi.org/10.5281/Zenodo

Iqbal, T., & Ali, H. (2018). Generative adversarial network for medical images (MI-GAN). *Journal of Medical Systems*, *42*(11), 231. https://doi.org/10.1007/s10916-018-1072-9

Isola, P., Zhu, J.-Y., Zhou, T., Efros, A. A., & Research, B. A. (2017). Image-to-image translation with conditional adversarial networks. *Proceedings of the IEEE Conference on Computer Vision and Pattern Recognition*, 1125–1134. https://doi.org/10.1109/cvpr.2017.632

Karamouz, M., Alipour, R. S., Roohinia, M., & Fereshtehpour, M. (2022). A remote sensing driven soil moisture estimator: Uncertain downscaling with geostatistically based use of ancillary data. *Water Resources Research*, *58*(10), e2022WR031946. https://doi.org/10.1029/2022wr031946

Kaur, A., & Sood, S. K. (2020). Deep learning based drought assessment and prediction framework. *Ecological Informatics*, *57*, 101067. https://doi.org/10.1016/j.ecoinf.2020.101067

Khan, N., Sachindra, D. A., Shahid, S., Ahmed, K., Shiru, M. S., & Nawaz, N. (2020). Prediction of droughts over Pakistan using machine learning algorithms. *Advances in Water Resources*, *139*, 103562. https://doi.org/10.1016/j.advwatres.2020.103562

Konapala, G., & Mishra, A. (2020). Quantifying climate and catchment control on hydrological drought in the continental United States. *Water Resources Research*, *56*(1). https://doi.org/10.1029/2018WR024620

Laloy, E., Hérault, R., Jacques, D., & Linde, N. (2018). Training-image based geostatistical inversion using a spatial generative adversarial neural network. *Water Resources Research*, *54*(1), 381–406. https://doi.org/10.1002/2017WR022148

Larraondo, P. R., Renzullo, L. J., Inza, I., & Lozano, J. A. (2019). A data-driven approach to precipitation parameterizations using convolutional encoder-decoder neural networks. *arXiv preprint arXiv:1903.10274*.

Li, C., & Wand, M. (2016). *Precomputed real-time texture synthesis with markovian generative adversarial networks. In: Leibe, B., Matas, J., Sebe, N., welling, M. (eds) computer Vision – ECCV 2016. ECCV 2016. Lecture notes in computer science* (Vol. 9907). Springer. https://doi.org/10.1007/978-3-319-46487-9_43

Li, J., Chen, Z., Cheng, L., & Liu, X. (2022). Energy data generation with wasserstein deep convolutional generative adversarial networks. *Energy*, *257*, 124694. https://doi.org/10.1016/j.energy.2022.124694

Li, J., Wang, Z., Wu, X., Xu, C. Y., Guo, S., Chen, X., & Zhang, Z. (2021). Robust meteorological drought prediction using antecedent SST fluctuations and machine learning. *Water Resources Research*, *57*(8). https://doi.org/10.1029/2020WR029413

Li, P., Ma, B., Palta, J. A., Ding, T., Cheng, Z., Lv, G., & Xiong, Y. (2021). Wheat breeding highlights drought tolerance while ignores the advantages of drought avoidance: A meta-analysis. *European Journal of Agronomy*, *122*, 126196. https://doi.org/10.1016/j.eja.2020.126196

Li, W., Xu, L., Liang, Z., Wang, S., Cao, J., Ma, C., & Cui, X. (2020). Sketch-then-edit generative adversarial network. *Knowledge-Based Systems*, *203*, 106102. https://doi.org/10.1016/j.knosys.2020.106102

Liu, C., Li, H., Su, A., Chen, S., & Li, W. (2021). Identification and grading of maize drought on RGB images of UAV based on improved U-Net. *IEEE Geoscience and Remote Sensing Letters*, *18*(2), 198–202. https://doi.org/10.1109/LGRS.2020.2972313

Liu, G., Shih, K. J., Wang, T. C., Reda, F. A., Sapra, K., Yu, Z., & Catanzaro, B. (2018). Partial convolution based padding. arXiv preprint arXiv:1811.11718. https://doi.org/10.48550/arXiv.1811.11718

Luebke, D. (2008). Cuda: Scalable parallel programming for high-performance scientific computing. In *2008 5th IEEE international symposium on biomedical imaging: From nano to macro* (pp. 836–838). IEEE. https://doi.org/10.1109/isbi.2008.4541126

Madadgar, S., & Moradkhani, H. (2013a). A Bayesian framework for probabilistic drought forecasting. *Journal of Hydrometeorology*, *14*, 1685–1705. https://doi.org/10.1175/JHM-D-13-010.1

Madadgar, S., & Moradkhani, H. (2013b). Drought analysis under climate change using copula. *Journal of Hydrologic Engineering*, *18*(7), 746–759. https://doi.org/10.1061/(ASCE)HE.1943-5584.0000532

Madadgar, S., & Moradkhani, H. (2014). Spatio-temporal drought forecasting within Bayesian networks. *Journal of Hydrology*, *512*, 134–146. https://doi.org/10.1016/j.jhydrol.2014.02.039

Markstrom, S. L., Hay, L. E., & Clark, M. P. (2016). Towards simplification of hydrologic modeling: Identification of dominant processes. *Hydrology and Earth System Sciences*, *20*(11), 4655–4671. https://doi.org/10.5194/hess-20-4655-2016

Mazrooei, A., & Sankarasubramanian, A. (2019). Improving monthly streamflow forecasts through assimilation of observed streamflow for rainfall-dominated basins across the CONUS. *Journal of Hydrology*, *575*, 704–715. https://doi.org/10.1016/j.jhydrol.2019.05.071

Minh Ngô, L., Karao, S., & Gevers, T. (2022). Self-supervised face image manipulation by conditioning GAN on face decomposition; self-supervised face image manipulation by conditioning GAN on face decomposition. *IEEE Transactions on Multimedia*, *24*, 2022. https://doi.org/10.1109/TMM.2021

Mitchell, K. E., Lohmann, D., Houser, P. R., Wood, E. F., Schaake, J. C., Robock, A., et al. (2004). The multi-institution North American Land Data Assimilation System (NLDAS): Utilizing multiple GCIP products and partners in a continental distributed hydrological modeling system. *Journal of Geophysical Research*, *109*(7). https://doi.org/10.1029/2003jd003823

Moeslund, J. E., Arge, L., Bøcher, P. K., Dalgaard, T., & Svenning, J. C. (2013). Topography as a driver of local terrestrial vascular plant diversity patterns. *Nordic Journal of Botany*, *31*(2), 129–144. https://doi.org/10.1111/j.1756-1051.2013.00082.x

Mokhtar, A., Jalali, M., He, H., Al-Ansari, N., Elbeltagi, A., Alsafadi, K., et al. (2021). Estimation of SPEI meteorological drought using machine learning algorithms. *IEEE Access*, *9*, 65503–65523. https://doi.org/10.1109/ACCESS.2021.3074305

Nie, F., Hu, Z., & Li, X. (2018). An investigation for loss functions widely used in machine learning. *Communications in Information and Systems*, *18*(1), 37–52. https://doi.org/10.4310/cis.2018.v18.n1.a2

NOAA/NIDIS. (2021). Winter 2020-21 in review: A look back at drought across the U.S. In 8 maps. NOAA/NIDIS. Retrieved from https://www.drought.gov/news/winter-2020-21-review-look-back-drought-across-us-8-maps

Nourani, V., Ghaneei, P., & Kantoush, S. A. (2022). Robust clustering for assessing the spatiotemporal variability of groundwater quantity and quality. *Journal of Hydrology*, *604*, 127272. https://doi.org/10.1016/j.jhydrol.2021.127272

Osman, M., Zaitchik, B. F., Badr, H. S., Christian, J. I., Tadesse, T., Otkin, J. A., & Anderson, M. C. (2021). Flash drought onset over the contiguous United States: Sensitivity of inventories and trends to quantitative definitions. *Hydrology and Earth System Sciences*, *25*(2), 565–581. https://doi.org/10.5194/hess-25-565-2021

Otkin, J. A., Anderson, M. C., Hain, C., Mladenova, I. E., Basara, J. B., & Svoboda, M. (2013). Examining rapid onset drought development using the thermal infrared-based evaporative stress index. *Journal of Hydrometeorology*, *14*(4), 1057–1074. https://doi.org/10.1175/JHM-D-12-0144.1

Otkin, J. A., Svoboda, M., Hunt, E. D., Ford, T. W., Anderson, M. C., Hain, C., & Basara, J. B. (2018). Flash droughts: A review and assessment of the challenges imposed by rapid-onset droughts in the United States. *Bulletin of the American Meteorological Society*, *99*(5), 911–919. https://doi.org/10.1175/BAMS-D-17-0149.1

Otkin, J. A., Zhong, Y., Hunt, E. D., Basara, J., Svoboda, M., Anderson, M. C., & Hain, C. (2019). Assessing the evolution of soil moisture and vegetation conditions during a flash drought-flash recovery sequence over the South-Central United States. *Journal of Hydrometeorology*, *20*(3), 549–562. https://doi.org/10.1175/JHM-D-18-0171.1

Pan, M., Sheffield, J., Wood, E. F., Mitchell, K. E., Houser, P. R., Schaake, J. C., et al. (2003). Snow process modeling in the North American land data assimilation system (NLDAS): 1. Evaluation of model simulated snow water equivalent. *Journal of Geophysical Research D: Atmospheres*, *108*(22). https://doi.org/10.1029/2003jd003994

Peters-Lidard, C. D., Kumar, S. v., Mocko, D. M., & Tian, Y. (2011). Estimating evapotranspiration with land data assimilation systems. *Hydrological Processes*, *25*(26), 3979–3992. https://doi.org/10.1002/hyp.8387

Radford, A., Metz, L., & Chintala, S. (2015). Unsupervised representation learning with deep convolutional generative adversarial networks. *arXiv preprint*.

Robic-Butez, P., & Win, T. Y. (2019). Detection of phishing websites using generative adversarial network. In *2019 IEEE international Conference on Big data (Big data)* (pp. 3216–3221). IEEE. https://doi.org/10.1109/bigdata47090.2019.9006352

Ronneberger, O., Fischer, P., & Brox, T. (2015). *U-Net: Convolutional networks for biomedical image segmentation. In: Navab, N., Hornegger, J., Wells, W., Frangi, A. (eds) Medical image computing and computer-assisted intervention – MICCAI 2015. MICCAI 2015. Lecture notes in computer science* (Vol. 9351). Springer. https://doi.org/10.1007/978-3-319-24574-4_28

Sarp, S., Kuzlu, M., Pipattanasomporn, M., & Guler, O. (2021). Simultaneous wound border segmentation and tissue classification using a conditional generative adversarial network. *Journal of Engineering*, *2021*(3), 125–134. https://doi.org/10.1049/tje2.12016

Sarp, S., Kuzlu, M., Wilson, E., & Guler, O. (2021). WG 2 an: Synthetic wound image generation using generative adversarial network. *Journal of Engineering*, *2021*(5), 286–294. https://doi.org/10.1049/tje2.12033

Sehgal, V., Gaur, N., & Mohanty, B. P. (2021). Global flash drought monitoring using surface soil moisture. *Water Resources Research*, *57*(9). https://doi.org/10.1029/2021WR029901

Sharghi, E., Nourani, V., Zhang, Y., & Ghaneei, P. (2022). Conjunction of cluster ensemble-model ensemble techniques for spatiotemporal assessment of groundwater depletion in semi-arid plains. *Journal of Hydrology*, *610*, 127984. https://doi.org/10.1016/j.jhydrol.2022.127984

Siddique, N., Paheding, S., Elkin, C. P., & Devabhaktuni, V. (2021). U-Net and its variants for medical image segmentation: A review of theory and applications. *IEEE Access*, *9*, 82031–82057. https://doi.org/10.1109/ACCESS.2021.3086020

Srivastava, N., Hinton, G., Krizhevsky, A., & Salakhutdinov, R. (2014). Dropout: A simple way to prevent neural networks from overfitting. *Journal of Machine Learning Research*, *15*.

Strachan, S., & Daly, C. (2017). Testing the daily PRISM air temperature model on semiarid mountain slopes. *Journal of Geophysical Research*, *122*(11), 5697–5715. https://doi.org/10.1002/2016JD025920

Su, J., Jin, Z., & Finkelstein, A. (2021). HiFi-GAN-2: Studio-quality speech enhancement via generative adversarial networks conditioned on acoustic features. *IEEE Workshop on Applications of Signal Processing to Audio and Acoustics, 2021-October*, 166–170. https://doi.org/10.1109/WASPAA52581.2021.9632770

Trebing, K., Stańczyk, T., & Mehrkanoon, S. (2021). SmaAt-UNet: Precipitation nowcasting using a small attention-UNet architecture. *Pattern Recognition Letters*, *145*, 178–186. https://doi.org/10.1016/j.patrec.2021.01.036

Tyagi, S., Zhang, X., Saraswat, D., Sahany, S., Mishra, S. K., & Niyogi, D. (2022). Flash drought: Review of concept, prediction and the potential for machine learning, deep learning methods. *Earth's Future*, *10*(11). https://doi.org/10.1029/2022ef002723

Varshney, M., & Singh, P. (2021). Optimizing nonlinear activation function for convolutional neural networks. *Signal, Image and Video Processing*, *15*(6), 1323–1330. https://doi.org/10.1007/s11760-021-01863-z

Vijayakumar, K., Kadam, V. J., & Sharma, S. K. (2021). Breast cancer diagnosis using multiple activation deep neural network. *Concurrent Engineering Research and Applications*, *29*(3), 275–284. https://doi.org/10.1177/1063293X211025105

Weyn, J. A., Durran, D. R., & Caruana, R. (2020). Improving data-driven global weather prediction using deep convolutional neural networks on a cubed sphere. *Journal of Advances in Modeling Earth Systems*, *12*(9), e2020MS002109. https://doi.org/10.1029/2020ms002109

Wilhite, D. A., Svoboda, M. D., & Hayes, M. J. (2007). Understanding the complex impacts of drought: A key to enhancing drought mitigation and preparedness. *Water Resources Management*, *21*(5), 763–774. https://doi.org/10.1007/s11269-006-9076-5

Williams, A. P., Cook, E. R., Smerdon, J. E., Cook, B. I., Abatzoglou, J. T., Bolles, K., et al. (2020). Large contribution from anthropogenic warming to an emerging North American megadrought. *Science*, *368*(6488), 314–318. https://doi.org/10.1126/science.aaz9600

Wrzesien, M. L., Pavelsky, T. M., Durand, M. T., Dozier, J., & Lundquist, J. D. (2019). Characterizing biases in mountain snow accumulation from global data sets. *Water Resources Research*, *55*(11), 9873–9891. https://doi.org/10.1029/2019WR025350

Wu, L., Tian, F., Xia, Y., Fan, Y., Qin, T., Lai, J., & Liu, T.-Y. (2018). Learning to teach with dynamic loss functions. *Advances in Neural Information Processing Systems*, *31*.

Xia, Y., Ek, M. B., Peters-Lidard, C. D., Mocko, D., Svoboda, M., Sheffield, J., & Wood, E. F. (2014). Application of USDM statistics in NLDAS-2: Optimal blended NLDAS drought index over the continental United States. *Journal of Geophysical Research*, *119*(6), 2947–2965. https://doi.org/10.1002/2013JD020994

Xia, Y., Hobbins, M. T., Mu, Q., & Ek, M. B. (2015). Evaluation of NLDAS-2 evapotranspiration against tower flux site observations. *Hydrological Processes*, *29*(7), 1757–1771. https://doi.org/10.1002/hyp.10299

Xia, Y., Mitchell, K., Ek, M., Sheffield, J., Cosgrove, B., Wood, E., et al. (2012). Continental-scale water and energy flux analysis and validation for the North American land data assimilation system project phase 2 (NLDAS-2): 1. Intercomparison and application of model products. *Journal of Geophysical Research*, *117*(3). https://doi.org/10.1029/2011JD016048

Xiao, C., Chen, N., Hu, C., Wang, K., Gong, J., & Chen, Z. (2019). Short and mid-term sea surface temperature prediction using time-series satellite data and LSTM-AdaBoost combination approach. *Remote Sensing of Environment*, *233*, 111358. https://doi.org/10.1016/j.rse.2019.111358

Xu, L., Abbaszadeh, P., Moradkhani, H., Chen, N., & Zhang, X. (2020). Continental drought monitoring using satellite soil moisture, data assimilation and an integrated drought index. *Remote Sensing of Environment*, *250*, 112028. https://doi.org/10.1016/j.rse.2020.112028

Xu, Z., Wang, S., Stanislawski, L. v., Jiang, Z., Jaroenchai, N., Sainju, A. M., et al. (2021). An attention U-Net model for detection of fine-scale hydrologic streamlines. *Environmental Modelling & Software*, *140*, 104992. https://doi.org/10.1016/j.envsoft.2021.104992

Yan, H., Zarekarizi, M., & Moradkhani, H. (2018). Toward improving drought monitoring using the remotely sensed soil moisture assimilation: A parallel particle filtering framework. *Remote Sensing of Environment*, *216*, 456–471. https://doi.org/10.1016/j.rse.2018.07.017

Yuan, X., Wang, Y., Ji, P., Wu, P., Sheffield, J., & Otkin, J. A. (2023). A global transition to flash droughts under climate change. *Science*, *380*(6641), 187–191. https://doi.org/10.1126/science.abn6301

Zarei, A. R., Mahmoudi, M. R., & Moghimi, M. M. (2022). Determining the most appropriate drought index using the random forest algorithm with an emphasis on agricultural drought. *Natural Hazards*, *115*(1), 923–946. https://doi.org/10.1007/s11069-022-05579-2

Zarekarizi, M., Yan, H., Ahmadalipour, A., & Moradkhani, H. (2021). A probabilistic framework for agricultural drought forecasting using the ensemble data assimilation and Bayesian multivariate modeling. *Global drought and flood: Observation, modeling, and prediction*, 147–164. https://doi.org/10.1002/9781119427339.ch8

Zeiler, M. D. (2012). Adadelta: An adaptive learning rate method. *arXiv preprint arXiv:1212.5701*. https://doi.org/10.48550/arXiv.1212.5701